dergone by the copper(II) complexes of *N*-(2-pyridylmethylidene)histidine in pyridine parallels that observed for the corresponding pyruvate complexes. This confirms our interpretation based on apical binding by the donor base, which causes a conformational inversion of the amino acid chelate ring to the conformation containing an equatorial side chain and an axial α-C–H bond,[4] and is in full agreement with Dunathan's prediction.[42] Racemization in pyridine is faster for complexes of type **21** than for those of type **4**. As for the reactions undergone by complexes of type **20** and **5**, the accelerating effect must be related to the presence of a higher positive charge.

Acknowledgment. This work was supported by the Italian CNR. We thank M. Bonfà for recording the NMR spectra and M. S. Franzoni for measuring the magnetic susceptibility of copper(II) complexes.

Registry No. **11**, 127-17-3; **12**, 3731-51-9; Zn(pyc-L-his)NO_3·H_2O, 86024-31-9; Zn(pyc-L-hisOCH_3)$(NO_3)_2$, 86045-51-4; Cu(pyc-L-his)ClO_4·H_2O, 86024-33-1; Cu(pyc-D-his)ClO_4·H_2O, 86087-49-2; Cu(pyc-L-hisOCH_3)$(ClO_4)_2$·H_2O, 86024-35-3; Cu(pyc-D-hisOCH_3)$(ClO_4)_2$·$HOCH_3$, 86024-37-5; Cu(pyc-L-his')·H_2O, 86024-38-6; Zn(pyc-L-ala)$^+$·H_2O, 86024-39-7; Zn(pyc-L-val)$^+$·H_2O, 86024-40-0; Zn(pyc-L-phe)$^+$·H_2O, 86024-41-1; Cu(pyc-L-ala)$^+$·H_2O, 86024-42-2; Cu(pyc-L-leu)$^+$·H_2O, 86024-43-3; Cu(pyc-L-val)$^+$·H_2O, 86024-44-4; Cu(pyc-L-phe)$^+$·H_2O, 86024-45-5; L-his, 71-00-1; D-his, 351-50-8; L-hisOCH_3, 1499-46-3; D-hisOCH_3, 17720-12-6; L-ala, 56-41-7; L-val, 72-18-4; L-phe, 63-91-2; L-leu, 61-90-5; 2-formylpyridine, 1121-60-4; α-ketoisovalerate, 759-05-7.

Supplementary Material Available: Listings of elemental analyses (Table I) and complete infrared data of zinc(II) and copper(II) complexes of histidine Schiff bases (Table II) (3 pages). Ordering information is given on any current masthead page.

(42) Dunathan, H. C. *Proc. Natl. Acad. Sci. U.S.A.* **1966**, *55*, 713–716.

Contribution from the Departments of Chemistry, Middle East Technical University, Ankara, Turkey, and Northern Illinois University, DeKalb, Illinois 60115

Ligand-to-Metal Charge-Transfer Spectra of Tetrahaloaurate(III) and *trans*-Dicyanodihaloaurate(III) Ions

HUSEYIN ISCI[1a] and W. ROY MASON*[1b]

Received November 24, 1982

Electronic absorption and magnetic circular dichroism (MCD) spectra are reported for AuX_4^- (X = Cl^-, Br^-), *trans*-$Au(CN)_2X_2^-$ (X = Cl^-, Br^-, I^-), and *trans*-$Au(CN)_2BrY^-$ (Y = Cl^-, I^-) in acetonitrile solution. These complexes exhibit a number of intense bands in the vis–UV region that are assigned to ligand-to-metal charge transfer (LMCT) from occupied halide-based orbitals to the lowest energy σ^* orbital, which is primarily $5d_{x^2-y^2}$ localized on gold. A detailed model for LMCT in planar complexes of D_{4h} and D_{2h} symmetries that includes halide spin–orbit coupling and intermixing σ- and π-bonding orbitals of the same symmetry is presented and used to interpret the absorption and MCD spectra.

Introduction

The intense bands exhibited by many halo complexes in the UV region have been assigned as ligand-to-metal charge-transfer (LMCT) electronic transitions.[2] Such transitions involve excitation of electrons from occupied orbitals localized on the halide to an empty or partly filled orbital of predominantly metal character, commonly a metal d orbital. The LMCT transitions can thus be viewed as an incipient reduction of the metal with concomitant oxidation of the halide ligand and are therefore related to the redox properties of the metal ion and halide. The low-energy LMCT excited states are also of considerable interest in the understanding of photochemical reactions of halo complexes.[3,4]

The study of the LMCT process in square-planar complexes based on investigation of typical Pt(II) halo complexes has been complicated by the presence of allowed metal 5d → 6p transitions in the same energy region as LMCT. For example, both d → p and LMCT assignments have been given to the intense band system near 4.4 μm^{-1} in $PtCl_4^{2-}$.[5-9] In contrast, the halo complexes of isoelectronic Au(III) are expected to be free of such complications because the 5d–6p energy separation is larger than for Pt(II). This together with the red shift expected for LMCT as the metal oxidation state is increased from Pt(II) to Au(III) ensures a large separation between d → p and LMCT band systems in Au(III). The study of Au(III) halo complexes therefore provides an excellent opportunity to characterize the LMCT process in square-planar complexes. However, apart from the $AuCl_4^-$ and $AuBr_4^-$ ions,[5,10-12] there have been few halo Au(III) complexes investigated and none in any great detail. Consequently, motivated by our general interest in LMCT in square-planar complexes, we describe herein a detailed model for low-energy LMCT excited states for the D_{4h} AuX_4^- ions. The model, which includes both intermixing of σ and π ligand orbitals of the same symmetries and consideration of halogen spin–orbit coupling, is used to interpret the electronic absorption and magnetic circular dichroism (MCD) spectra for $AuCl_4^-$ and $AuBr_4^-$ that were obtained in acetonitrile solution. Although aqueous MCD spectra for these ions were reported earlier,[5] they have been carefully remeasured with high sensitivity here in acetonitrile. Also a low-temperature (ca. 15 K) MCD measurement was made for $HAuCl_4$ incorporated into a thin transparent poly(vinyl alcohol) (PVA) film. In addition the LMCT model generalized to D_{2h} symmetry is used to interpret

(1) (a) Middle East Technical University. (b) Northern Illinois University.
(2) See for example: (a) Jørgensen,, C. K. "Absorption Spectra and Chemical Bonding in Complexes"; Addison-Wesley: Reading, MA, 1962. (b) Ballhausen, C. J.; Gray, H. B. In "Coordination Chemistry"; Martell, A. F., Ed.; American Chemical Society: Washington, DC, 1971; ACS Monogr. No. 168, p 3.
(3) Balzani, V.; Carassiti, V. "Photochemistry of Coordination Compounds"; Academic Press: New York, 1970.
(4) Wrighton, M. S. *Top. Curr. Chem.* **1976**, *65*, 37.
(5) McCaffery, A. J.; Schatz, P. N.; Stephens, P. J. *J. Am. Chem. Soc.* **1968**, *90*, 5730.
(6) Chatt, J.; Gamlen, G. A.; Orgel, L. E. *J. Chem. Soc.* **1958**, 486.
(7) Mason, W. R.; Gray, H. B. *J. Am. Chem. Soc.* **1968**, *90*, 5721.
(8) Anex, B. G.; Takeuchi, N. *J. Am. Chem. Soc.* **1974**, *96*, 4411.
(9) Elding, L. I.; Olsson, L. F. *J. Phys. Chem.* **1978**, *82*, 69.
(10) Mason, W. R.; Gray, H. B. *Inorg. Chem.* **1968**, *7*, 55.
(11) Schwartz, R. W. *Inorg. Chem.* **1977**, *16*, 836.
(12) Brown, D. H.; Smith, W. E. *J. Chem. Soc., Dalton Trans.* **1976**, 848.

0020-1669/83/1322-2266$01.50/0

some new absorption and MCD measurements for *trans*-$Au(CN)_2X_2^-$ ($X = Cl^-, Br^-, I^-$) in acetonitrile solution. Solution absorption spectra in acetonitrile are also reported for *trans*-$Au(CN)_2BrY^-$ ($Y = Cl^-, I^-$). In the case of these halocyano complexes the cyano ligands have very stable filled orbitals and are expected to be transparent in the halide LMCT spectral region. Further, Au(III) to CN^- charge transfer is considered unlikely due to the stability of the occupied 5d orbitals of Au(III). Thus for example $Au(CN)_4^-$ has no maxima or shoulder absorptions below 5.2 μm^{-1} [10] whereas *trans*-$Au(CN)_2X_2^-$ ($X = Cl^-, Br^-$) and *trans*-$Au(CN)_2BrCl^-$ are known[13,14] to exhibit intense bands in the UV below 5.2 μm^{-1}, which are presumably halide to gold LMCT, though detailed assignments have not been made. The trans configuration for the $Au(CN)_2X_2^-$ ions was assigned on the basis of infrared and Raman spectra.[15,16]

Experimental Section

Preparation of Compounds. The preparation of $[(n\text{-}C_4H_9)_4N][AuX_4]$ ($X = Cl^-, Br^-$) has been described earlier.[10] The *trans*-dihalodicyanoaurate(III) complexes were prepared by reacting $KAu(CN)_2$ with halogen in aqueous methanol.[16] Tetra-*n*-butylammonium salts were precipitated upon addition of a concentrated aqueous solution of $[(n\text{-}C_4H_9)_4N]X$ for *trans*-$Au(CN)_2X_2^-$ ($X = Cl^-, Br^-$) or of $[(n\text{-}C_4H_9)_4N]Cl$ for *trans*-$Au(CN)_2I_2^-$. Yields were better than 90%, and all compounds gave good elemental analysis. The $[(n\text{-}C_4H_9)_4N][Au(CN)_2BrI]$ salt was prepared by mixing equimolar solutions of $[(n\text{-}C_4H_9)_4N][Au(CN)_2X_2]$ ($X = Br^-, I^-$) in dichloromethane and evaporating the solvent. The compound gave good elemental analysis and contained intense lines in an X-ray powder pattern that were absent in the powder patterns of either of the starting compounds. The preparation and analyses of $K[Au(CN)_2Br_2]$ and $[(CH_3)_4N][Au(CN)_2BrCl]$ have been given previously.[13]

Spectral Measurements. Electronic absorption spectra were determined with a Cary 1501 or a Cary 17D spectrophotometer. MCD measurements at 1 T were made with a JASCO ORD/UV-5 (equipped with a CD attachment and a permanent magnet), and measurements at 7 T were made on a computer-controlled spectrometer built at Northern Illinois University[17] equipped with a superconducting magnet (Oxford Instruments SM2-7). The 7-T MCD measurements featured simultaneous, synchronous measurement of the absorption spectra along a common light path and MCD signal to noise approximately 200 times better than the 1-T measurements. Absorption spectra at 77 K were obtained by immersing transparent poly(vinyl alcohol) (PVA) films containing the complex into liquid nitrogen in a quartz dewar situated in the light beam of the spectrophotometer. Low-temperature MCD (ca. 15 K) measurements were obtained by mounting a strain-free PVA film in the variable-temperature insert of the magnet bore and cooling with liquid helium.

Determination of Dissociation Constants for *trans*-$Au(CN)_2I_2^-$ and *trans*-$Au(CN)_2BrI^-$. The solution spectra of *trans*-$Au(CN)_2I_2^-$ and *trans*-$Au(CN)_2BrI^-$ in acetonitrile did not obey Beer's law, and absorption bands characteristic of $Au(CN)_2^-$ were observed. This behavior is interpreted as halogen dissociation, given for example for *trans*-$Au(CN)_2I_2^-$:

$$\textit{trans}\text{-}Au(CN)_2I_2^- \rightleftharpoons Au(CN)_2^- + I_2$$

The dissociation constant K is given by

$$K = [Au(CN)_2^-][I_2]/[Au(CN)_2I_2^-] = x(x + a)/(C_0 - x)$$

where C_0 is the initial Au(III) concentration, x is the equilibrium concentration of I_2, and a is the added $Au(CN)_2^-$ concentration. Dissociation constants for *trans*-$Au(CN)_2I_2^-$ and *trans*-$Au(CN)_2BrI^-$ were determined by measuring the absorbance at the band maxima at 3.67 and 3.89 μm^{-1}, respectively, as a function of added $Au(CN)_2^-$ or C_0. In both cases the band intensity became independent of $[Au(CN)_2^-]$ when the $[Au(CN)_2^-]/C_0$ ratio was ≥ 10. Under conditions of excess $Au(CN)_2^-$, x may be taken as 0 and the absorptivity of the band maxima for the Au(III) complexes determined. Once the absorptivity of the Au(III) complex is known, x may be determined for a known [Au(III)] from $C_0 - x$ and K values for concentrations of added $Au(CN)_2^-$ computed. These data are collected in Table I. Values for *trans*-$Au(CN)_2I_2^-$ were self-consistent to within ±7%; those for *trans*-$Au(CN)_2BrI^-$ were less precise.

Table I. Dissociation Constants in CH_3CN at 23 °C

10^5C_0, M	10^5x, M	10^5a, M	10^6K, M
	trans-$Au(CN)_2I_2^-$		
2.16	0.854	0	5.6
2.21	0.418	2.28	6.3
2.21	0.218	5.37	6.1
	trans-$Au(CN)_2BrI^-$		
3.66	0.404	0	0.5
7.33	0.718	0	0.8

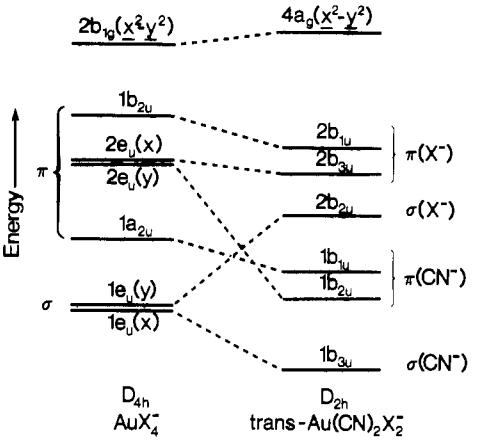

Figure 1. Relative energy of spectroscopically important one-electron MO's in D_{4h} and D_{2h} halo complexes. Occupied Au(III) 5d orbitals are omitted for clarity.

The measured dissociation constants were used to correct the observed spectra for *trans*-$Au(CN)_2I_2^-$ and *trans*-$Au(CN)_2BrI^-$ solutions. The corrections were relatively small (<15%) for the more concentrated ($\geq 2 \times 10^4$ M) solutions used for the low-energy absorptions but were larger for the more dilute solutions necessary at higher energy. Above 4.0 μm^{-1}, both I_2 and $Au(CN)_2^-$ absorb strongly and the corrected spectra required subtractions of their contribution to the observed spectra. Therefore, the corrected spectra at high energy may be less accurate, as noted in the spectral data table, Table IV.

Computations. Spin–orbit eigenvalues and eigenvectors for allowed E_u and A_{2u} excited states of AuX_4^- were computed by diagonalizing the appropriate E_u and A_{2u} secular determinants (see Table III). These calculations involved a range of σ–π mixing and halogen spin–orbit coupling ζ_{np} parameters. However, since the number of observable absorption bands in the spectra of the complex ions is considerably smaller than the number of input energies required, the calculations were not unique and were only used as "models" to explore the effect of changes in σ–π mixing and spin–orbit interaction on the E_u and A_{2u} states.

Experimental MCD A_1 and B_0 terms were determined from a moment analysis[18] of the MCD spectra for AuX_4^-. The average energy about which the analysis was performed, $\bar{\nu}_0$, was obtained by setting the first moment of the absorption to zero. A_1 terms were evaluated from $\int(\Delta\epsilon_M/\bar{\nu})(\bar{\nu} - \bar{\nu}_0)\,d\bar{\nu} = \langle\Delta\epsilon_M\rangle_1 = 152.5A_1$; B_0 terms were evaluated from $\int(\Delta\epsilon_M/\bar{\nu})\,d\bar{\nu} = \langle\Delta\epsilon_M\rangle_0 = 152.5B_0$; the value of D_0 was determined from $\int(\epsilon/\bar{\nu})\,d\bar{\nu} = \langle\epsilon\rangle_0 = 326.6D_0$. The quantity $\Delta\epsilon_M$ is the differential molar absorptivity per unit magnetic field with units $(M\ cm\ T)^{-1}$.

Molecular Orbitals and LMCT States

Figure 1 shows the one-electron MO energy levels for AuX_4^- (D_{4h}) and *trans*-$Au(CN)_2X_2^-$ (D_{2h}) that will be helpful in visualizing the MLCT excited configurations. For both types

(13) Mason, W. R. *Inorg. Chem.* **1970**, *9*, 2688.
(14) Gupta, S. *Naturwissenschaften* **1968**, *55*, 442.
(15) Jones, L. H. *Inorg. Chem.* **1964**, *3*, 1581.
(16) Smith, J. M.; Jones, L. H.; Kressin, I. K.; Penneman, R. A. *Inorg. Chem.* **1965**, *4*, 369.
(17) Mason, W. R. *Anal. Chem.* **1982**, *54*, 646.
(18) Stephens, P. J. *Adv. Chem. Phys.* **1976**, *35*, 197.

Table II. LMCT Excited Configurations and States

config[a]	type	no spin–orbit coupling	spin–orbit states[b]
		D_{4h}: AuX_4^-	
$(1b_{2u})(2b_{1g})$	$n \rightarrow \sigma^*$	$^1A_{2u}$	A_{2u}
		$^3A_{2u}$	E_u (A_{1u})
$(2e_u')^3(2b_{1g})$	$\pi \rightarrow \sigma^*$	b^1E_u	E_u
		b^3E_u	E_u, A_{2u} (A_{1u}, B_{1u}, B_{2u})
$(1a_{2u})(2b_{1g})$	$\pi \rightarrow \sigma^*$	$^1B_{2u}$	(B_{2u})
		$^3B_{2u}$	(B_{2u}), E_u (A_{1u})
$(1e_u')^3(2b_{1g})$	$\sigma \rightarrow \sigma^*$	a^1E_u	E_u
		a^3E_u	E_u, A_{2u} (A_{1u}, B_{1u}, B_{2u})
		D_{2h}: *trans*-$Au(CN)_2X_2^-$	
$(2b_{1u})(4a_g)$	$\pi \rightarrow \sigma^*$	$^1B_{1u}$	B_{1u}
		$^3B_{1u}$	B_{2u}, B_{3u} (A_u)
$(2b_{3u}')(4a_g)$	$\pi \rightarrow \sigma^*$	$^1B_{3u}$	B_{3u}
		$^3B_{3u}$	B_{1u}, B_{2u} (A_u)
$(2b_{2u}')(4a_g)$	$\sigma \rightarrow \sigma^*$	$^1B_{2u}$	B_{2u}
		$^3B_{2u}$	B_{1u}, B_{3u} (A_u)

[a] Filled orbitals are omitted; the primed orbitals indicate σ–π mixed orbitals of eq 1–4 (see text). [b] Forbidden states are given in parentheses.

of complex the z axis is taken perpendicular to the molecular plane, and in the case of the D_{2h} complexes the X^- ligands lie on the y axis. Both types of complex have only filled orbitals below the empty metal-based (largely gold 5d) $2b_{1g}(x^2 - y^2)$ or $4a_g(x^2 - y^2)$ orbital, and hence their ground states are diamagnetic and nondegenerate and are designated $^1A_{1g}$ or ^1A_g, respectively. The lowest energy excited LMCT configurations involve excitations to the $2b_{1g}(x^2 - y^2)$ or $4a_g(x^2 - y^2)$ σ^* orbital, and these excitations may be loosely classified into three types: $n \rightarrow \sigma^*$ (D_{4h} only) $1b_{2u} \rightarrow 2b_{1g}(x^2 - y^2)$; $\pi \rightarrow \sigma^*$ (D_{4h}) $2e_u \rightarrow 2b_{1g}(x^2 - y^2)$ and $1a_{2u} \rightarrow 2b_{1g}(x^2 - y^2)$, ($D_{2h}$) $2b_{1u} \rightarrow 4a_g(x^2 - y^2)$ and $2b_{3u} \rightarrow 4a_g(x^2 - y^2)$; and $\sigma \rightarrow \sigma^*$ (D_{4h}) $1e_u \rightarrow 2b_{1g}(x^2 - y^2)$, ($D_{2h}$) $2b_{2u} \rightarrow 4a_g(x^2 - y^2)$. On the basis of overlap considerations that lead to the prediction of small dipole strengths for $\pi \rightarrow \sigma^*$ type transitions compared to large dipole strengths expected for $\sigma \rightarrow \sigma^*$ transitions, Jørgensen[2a,19] and others[20] have argued cogently for extensive intermixing of σ and π of one-electron orbitals of the same symmetry. This σ–π mixing allows for reasonable intensity for $\pi \rightarrow \sigma^*$ transitions in a variety of octahedral hexahalo complexes.[20] Aplication of σ–π mixing to planar halo complexes was suggested for the same reasons as for octahedral systems.[5,21] Thus for the D_{4h} complexes, the σ–π mixing would involve the $1e_u\sigma$ and $2e_u\pi$ orbitals with the result that two new "mixed" orbitals would be formed in eq 1 and 2 (λ_1 and λ_2 are mixing coefficients such that $\lambda_1, \lambda_2 > 0$ and $\lambda_1^2 + \lambda_2^2 = 1$). Analogous σ–π mixing for the D_{2h} complexes will involve the $2b_{2u}\sigma$ and $2b_{3u}\pi$ X^- orbitals and the $1b_{3u}\sigma$ and $1b_{2u}\pi$ CN^- orbitals:

$$1e_u'\sigma = \lambda_1(1e_u\sigma) + \lambda_2(2e_u\pi) \quad (1)$$

$$2e_u'\pi = -\lambda_2(1e_u\sigma) + \lambda_1(2e_u\pi) \quad (2)$$

$$\begin{aligned} 2b_{3u}'\pi &= -\lambda_4(1b_{3u}\sigma) + \lambda_3(2b_{3u}\sigma) \\ 1b_{2u}'\pi &= \lambda_6(2b_{2u}\sigma) + \lambda_5(1b_{2u}\pi) \\ 2b_{2u}'\sigma &= \lambda_5(2b_{2u}\sigma) - \lambda_6(1b_{2u}\pi) \\ 1b_{3u}'\sigma &= \lambda_3(1b_{3u}\sigma) + \lambda_4(2b_{3u}\pi) \end{aligned} \quad (3)$$

$$1b_{3u}'\sigma = \lambda_3(1b_{3u}\sigma) + \lambda_4(2b_{3u}\pi) \quad (4)$$

With these σ–π mixed orbitals, together with the unmixed $1b_{2u}$ and $1a_{2u}$ in D_{4h} or $2b_{1u}$ in D_{2h}, the excited configurations and low-energy LMCT excited states are constructed and are collected in Table II.

For heavy-metal complexes containing heavy-atom ligands spin–orbit interaction must also be considered. Since the LMCT configurations visualized here each involve excitation to a single nondegenerate metal-based orbital, metal spin–orbit coupling can be neglected. Ligand spin–orbit coupling however will increase in the order $Cl^- < Br^- < I^-$ (ζ_{3p} for Cl = 587 cm^{-1}, ζ_{4p} for Br = 2457 cm^{-1}, and ζ_{5p} for I = 5069 cm^{-1}),[2a,19] and significant spin–orbit effects are expected for bromo and iodo complexes. Strong halogen spin–orbit coupling will serve to mix singlet and triplet states within the excited LMCT configurations of Table II. The symmetries of the spin–orbit states expected for each LMCT configuration are also listed in Table II. Since electric dipole selection rules dictate that only transitions to A_{2u} (z-polarized) or E_u (x,y-polarized) states for D_{4h} and B_{1u} (z-polarized), B_{2u} (y-polarized), or B_{3u} (x-polarized) states for D_{2h} will be allowed, only the coupling among these states respectively need be considered. Forbidden transitions to A_{1u}, B_{1u}, or B_{2u} states in D_{4h} or A_u in D_{2h} will be very weak and likely will be obscured by the more intense allowed transitions. The quantitative treatment of spin–orbit coupling requires diagonalization of appropriate spin–orbit secular determinants for the six E_u and three A_{2u} states of D_{4h} and the three each B_{1u}, B_{2u}, and B_{3u} states of D_{2h}. The secular determinants, which include provision for σ–π mixing, are listed in Table III. In the evaluation of the matrix elements for these determinants, the relevant orbitals were approximated as pure halogen np or pure gold 5d orbitals, and only one-centered integrals were retained (contributions from two-centered integrals are expected to be small). The diagonalization of these determinants requires energies for singlet and triplet LMCT states in the absence of spin–orbit coupling, the σ–π mixing coefficients, and the halogen ζ_{np} parameter as input. The diagonalized determinants give spin–orbit eigenvalues and eigenvectors. The E_u and A_{2u} eigenvectors will be of the form in eq 5 and 6 (a_i–l_i are coefficients determined by the diagonalization). The B_{1u}, B_{2u}, and B_{3u} eigenvectors are formulated similarly in eq 7–9.

$$|E_u(i)\rangle = a_i|E_u(^3A_{2u})\rangle + b_i|E_u(b^1E_u)\rangle + c_i|E_u(b^3E_u)\rangle + d_i|E_u(^3B_{2u})\rangle + e_i|E_u(a^1E_u)\rangle + f_i|E_u(a^3E_u)\rangle \quad (5)$$

$$|A_{2u}(i)\rangle = g_i|A_{2u}(^1A_{2u})\rangle + h_i|A_{2u}(b^3E_u)\rangle + l_i|A_{2u}(a^3E_u)\rangle \quad (6)$$

$$|B_{1u}(i)\rangle = a_i|B_{1u}(^1B_{1u})\rangle + b_i|B_{1u}(^3B_{2u})\rangle + c_i|B_{1u}(^3B_{3u})\rangle \quad (7)$$

$$|B_{2u}(i)\rangle = d_i|B_{2u}(^3B_{1u})\rangle + e_i|B_{2u}(^1B_{2u})\rangle + f_i|B_{2u}(^3B_{3u})\rangle \quad (8)$$

$$|B_{3u}(i)\rangle = g_i|B_{3u}(^3B_{1u})\rangle + h_i|B_{3u}(^3B_{2u})\rangle + l_i|B_{3u}(^1B_{3u})\rangle \quad (9)$$

MCD Terms.[18] In order to properly interpret the MCD spectra of the halo Au(III) complexes investigated here, the A_1 and B_0 terms expected for the allowed LMCT transitions were derived (the complexes are diamagnetic so C_0 terms will be absent).

For the D_{4h} complexes the A_1 terms for each degenerate $E_u(j)$ state will be given by eq 10,[18] where L_z and S_z are orbital

$$A_1(j) = i\langle E_u(j)x|L_z + 2S_z|E_u(j)y\rangle D_0(^1E_u) \quad (10)$$

and spin angular momentum operators in the z direction and $D_0(^1E_u) = |D(^1E_u)|^2 = |3^{-1/2}\langle ^1A_{1g}|\mathbf{m}|^1E_u\rangle|^2$, the dipole strength of a fully allowed $^1A_{1g} \rightarrow {}^1E_u$ transition, taken here to be the pure σ–σ^* transition. By substitution of eq 5 into eq 10 and retention of only one-centered integrals, the following expression results after simplification:

$$A_1(i) \simeq 2[|a_i|^2 - |d_i|^2 + \lambda_1\lambda_2(-|b_i|^2 - |c_i|^2 + |e_i|^2 + |f_i|^2) + \tfrac{1}{2}(\lambda_1^2 - \lambda_2^2)(b_i^*e_i + c_i^*f_i + e_i^*b_i + f_i^*c_i)] \times |b_i(-\lambda_2) + e_i(\lambda_1)|^2|D(^1E_u)|^2 \quad (11)$$

The B_0 terms are more difficult to evaluate because they

(19) Jørgensen, C. K. *Mol. Phys.* **1959**, *2*, 309.
(20) Henning, G. N.; Dobosh, P. A.; McCaffery, A. J.; Schatz, P. N. *J. Am. Chem. Soc.* **1970**, *92*, 5377.
(21) Reference 2a, p 199.

Table III. Spin-Orbit Secular Determinants (Upper Triangles)

symmetry	determinant[a]
	D_{4h}: AuX_4^-
A_{2u}	$\begin{vmatrix} {}^1A_{2u}-E & -\frac{1}{2}(\lambda_1-\lambda_2)i\zeta & -\frac{1}{2}(\lambda_1+\lambda_2)i\zeta \\ & b^3E_u-\lambda_1\lambda_2\zeta-E & \frac{1}{2}(\lambda_1^2+\lambda_2^2)\zeta \\ & & a^3E_u+\lambda_1\lambda_2\zeta-E \end{vmatrix}$
E_u	$\begin{vmatrix} {}^3A_{2u}-E & -8^{-1/2}(\lambda_1-\lambda_2)i\zeta & -8^{-1/2}(\lambda_1-\lambda_2)\zeta & 0 & -8^{-1/2}(\lambda_1+\lambda_2)i\zeta & -8^{-1/2}(\lambda_1+\lambda_2)\zeta \\ & b^1E_u-E & \lambda_1\lambda_2 i\zeta & -8^{-1/2}(\lambda_1+\lambda_2)\zeta & 0 & -\frac{1}{2}(\lambda_1^2-\lambda_2^2)i\zeta \\ & & b^3E_u-E & -8^{-1/2}(\lambda_1+\lambda_2)\zeta & \frac{1}{2}(\lambda_1^2-\lambda_2^2)i\zeta & 0 \\ & & & {}^3B_{2u}-E & -8^{-1/2}(\lambda_1-\lambda_2)i\zeta & 8^{-1/2}(\lambda_1-\lambda_2)\zeta \\ & & & & a^1E_u-E & -\lambda_1\lambda_2 i\zeta \\ & & & & & a^3E_u-E \end{vmatrix}$
	D_{2h}: *trans*-$Au(CN)_2X_2^-$
B_{1u}	$\begin{vmatrix} {}^1B_{1u}-E & \frac{1}{2}\lambda_5 i\zeta & \frac{1}{2}\lambda_3 i\zeta \\ & {}^3B_{2u}-E & \frac{1}{2}\lambda_3\lambda_5\zeta \\ & & {}^3B_{3u}-E \end{vmatrix}$
B_{2u}	$\begin{vmatrix} {}^3B_{1u}-E & \frac{1}{2}\lambda_5 i\zeta & -\frac{1}{2}\lambda_3\zeta \\ & {}^1B_{2u}-E & \frac{1}{2}\lambda_3\lambda_5 i\zeta \\ & & {}^3B_{3u}-E \end{vmatrix}$
B_{3u}	$\begin{vmatrix} {}^3B_{1u}-E & \frac{1}{2}\lambda_5\zeta & \frac{1}{2}\lambda_3 i\zeta \\ & {}^3B_{2u}-E & \frac{1}{2}\lambda_3\lambda_5 i\zeta \\ & & {}^1B_{3u}-E \end{vmatrix}$

[a] Energies of excited states in the absence of spin-orbit coupling appear along the diagonal; ζ is the halogen ζ_{np} spin-orbit coupling constant; λ_1-λ_5 are σ-π mixing coefficients of eq 1-4.

require summations over all electronic states of the molecule, eq 12,[18] where mixing with the ground state a has been assumed to be negligible. However because of the inverse dependence on the energy difference $W_k - W_j$, between the state of interest (j) and all other states (k) mixed by the field, B_0 terms can be approximated by limiting the summation to include only those states that lie close in energy. Thus for a LMCT transition in the UV the summation can be limited to include only the *other* LMCT excited states. The B_0 terms for D_{4h} can be approximated as

$$B_0(a \rightarrow j) = -\tfrac{2}{3}i\sum(W_k - W_j)^{-1}\langle j|\mathbf{L} + 2\mathbf{S}|k\rangle\cdot\langle a|\mathbf{m}|j\rangle\mathbf{x}\langle k|\mathbf{m}|a\rangle \quad (12)$$

$$B_0[E_u(j)] = \sum B_0(E_u,E_u)_{jk} + \sum B_0(E_u,A_{2u})_{jk}$$

and

$$B_0[A_{2u}(j)] = \sum B_0(E_u,A_{2u})_{jk}$$

where k ranges over all the $E_u(i)$ and $A_{2u}(i)$ LMCT states and $B_0(E_u,E_u)_{jk}$ and $B_0(E_u,A_{2u})_{jk}$ are given by eq 13 and 14. In

$$B_0(E_u,E_u)_{jk} = -2(W_k - W_j)^{-1}[2a_j^*a_k - 2d_j^*d_k - 2\lambda_1\lambda_2(b_j^*b_k + c_j^*c_k - e_j^*e_k - f_j^*f_k) + (\lambda_1^2 - \lambda_2^2)(b_j^*e_k + c_j^*f_k + e_j^*b_k + f_j^*c_k)][b_j(-\lambda_2) + e_j(\lambda_1)] \times [b_k(-\lambda_2) + e_k\lambda_1]^*|D(^1E_u)|^2 \quad (13)$$

$$B_0(E_u,A_{2u})_{jk} = -2(W_k - W_j)^{-1}[-2c_j^*h_k - 2f_j^*l_k - \tfrac{1}{2}(\lambda_1 + \lambda_2)(2^{1/2}e_j^*g_k + d_j^*h_k - a_j^*l_k) - \tfrac{1}{2}(\lambda_1 - \lambda_2)(2^{1/2}b_j^*g_k - a_j^*h_k - d_j^*l_k)][b_j(-\lambda_2) + e_j(\lambda_1)](g_k^*)(D(^1E_u y))(D^*(^1A_{2u})) \quad (14)$$

eq 14 $D(^1E_u y) = 3^{-1/2}\langle {}^1A_{1g}|m_y|{}^1E_u y\rangle$, $D(^1A_{2u}) = 3^{-1/2}\langle {}^1A_{1g}|m_z|{}^1A_{2u}\rangle$, and use is made of the relations $B_0(E_u,E_u)_{kj} = -B_0(E_u,E_u)_{jk}$ and $B_0(A_{2u},E_u)_{kj} = -B_0(E_u,A_{2u})_{jk}$.

For the D_{2h} complexes only B_0 terms are expected since there are no degenerate states. Expressions similar to eq 13 and 14 can be developed for the B_{1u}, B_{2u}, and B_{3u} LMCT states. For example

$$B_0[B_{3u}(j)] = \sum B_0(B_{3u},B_{1u})_{jk} + \sum B_0(B_{3u},B_{2u})_{jk}$$

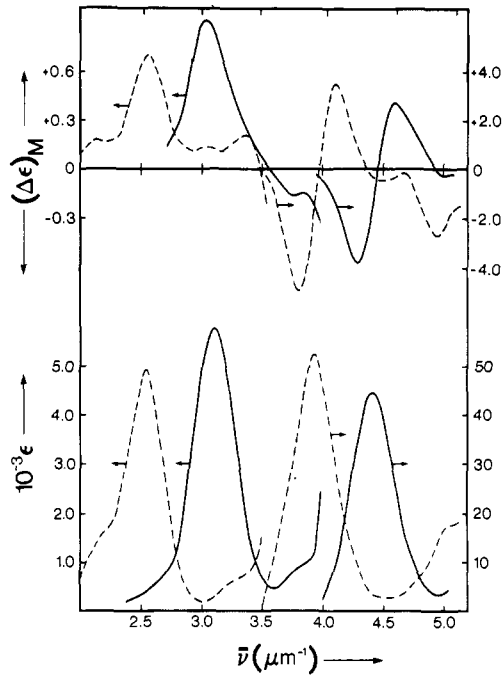

Figure 2. Absorption (lower curves) and MCD (upper curves) spectra for $[(n\text{-}C_4H_9)_4N][AuX_4]$ in CH_3CN solution: —, X = Cl^-; ---, X = Br^-.

with similar expressions for $B_0[B_{1u}(j)]$ and $B_0[B_{2u}(j)]$. The $B_0(B_{3u},B_{1u})_{jk}$ and $B_0(B_{3u},B_{2u})_{jk}$ terms are given by

$$B_0(B_{3u},B_{1u})_{jk} = -2(W_k - W_j)^{-1}(\lambda_3 l_j^*a_k - 2h_j^*b_k - \lambda_3 g_j^*c_k) \times (l_j a_k^*)(D(^1B_{3u}))(D(^1B_{1u})^*) \quad (15)$$

$$B_0(B_{3u},B_{2u})_{jk} = -2(W_k - W_j)^{-1}[-2g_j^*d_k - \lambda_3\lambda_5 l_j^*e_k + \lambda_3\lambda_5 h_j^*f_k](l_j e_k^*)(D(^1B_{3u}))(D(^1B_{2u})^*) \quad (16)$$

where the coefficients a_k, l_j, etc. refer to eq 7-9.

Absorption and MCD Spectra

Figures 2-4 present typical absorption and MCD spectra for acetonitrile solution. Detailed spectral data are collected in Table IV. In addition to the acetonitrile solution results,

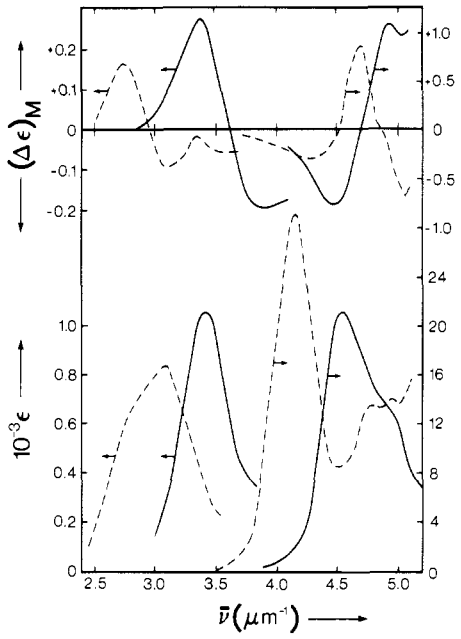

Figure 3. Absorption (lower curves) and MCD (upper curves) spectra for *trans*-$Au(CN)_2X_2^-$ in CH_3CN solution: —, X = Cl^-; - - -, X = Br^-.

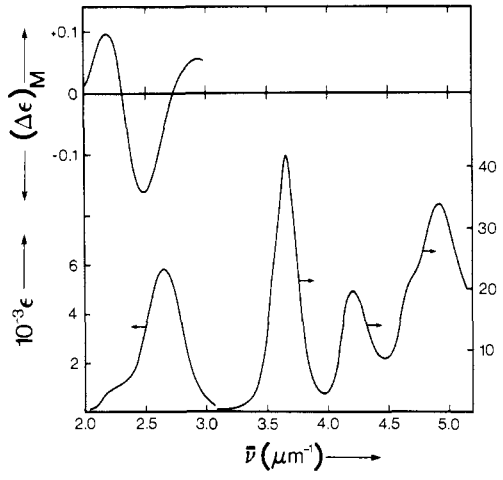

Figure 4. Absorption (lower curves) and MCD (upper curve) spectra for *trans*-$Au(CN)_2I_2^-$ in CH_3CN solution. Absorption spectra were corrected for I_2 dissociation (see text).

low-temperature (ca. 15 K) absorption and MCD measurements were made for $AuCl_4^-$ in a PVA film. Some enhancement in resolution of the shoulder absorptions was noted, but the results were rather similar to the room-temperature solution results. Similarly, 77 K PVA absorption spectra for *trans*-$Au(CN)_2Cl_2^-$ and *trans*-$Au(CN)_2Br_2^-$ were obtained; again some narrowing of the bands was noted, but the results were only slightly improved over the room-temperature measurements. The temperature dependence of the spectra in all cases was consistent with allowed transitions in the region of interest.

As explained in the Experimental Section, the halogen dissociation complicated the measurements for *trans*-$Au(CN)_2I_2^-$ and *trans*-$Au(CN)_2BrI^-$. The spectrum presented in Figure 4 and the data in Table IV represent spectra corrected for the dissociation equilibrium. Because the corrections above 4.0 μm^{-1} were substantial and the absorptions due to I_2 and $Au(CN)_2^-$ were large, the data in this region may be less accurate.

Efforts were made to obtain MCD data for *trans*-$Au(CN)_2I_2^-$ in the region of band III at 3.67 μm^{-1}, but the signal to noise was unfavorable at the high sensitivity required. The MCD is very weak in this region; $\Delta\epsilon$ at 3.67 μm^{-1} was less than 0.06 $(M\ cm\ T)^{-1}$.

Table IV. Spectral Data[a]

band no.	absorption λ, nm	absorption $\bar{\nu}$, μm^{-1} (ϵ, $M^{-1}\ cm^{-1}$)	MCD $\bar{\nu}$, μm^{-1} ($\Delta\epsilon_M$, $M^{-1}\ cm^{-1}\ T^{-1}$)	excited state assignt
		$[(n\text{-}C_4H_9)_4N][AuCl_4]$		
I	323	3.10 (5800)	3.04 (+0.91)	$E_u(b^1E_u)$, $A_{2u}(^1A_{2u})$
II	263[b]	3.80 (880)	3.76 (−0.16)	$B_{2u}(^1B_{2u})$
III	227	4.41 (44 800)	c 4.28 (−3.84); 4.45 (0); 4.60 (+2.67)	$E_u(a^1E_u)$
		$[(n\text{-}C_4H_9)_4N][AuBr_4]$		
I	476[b]	2.10 (1230)	2.12 (+0.18)	$E_u(^3A_{2u})$, A_{2u}, $E_u(^3E_u)$
II	394	2.54 (4900)	2.56 (+0.71)	$E_u(b^1E_u)$, $A_{2u}(^1A_{2u})$
			3.04 (+0.13)	$E_u(^3B_{2u})$
III	303[b]	3.30 (660)	3.39 (+0.20)	$B_{2u}(^1B_{2u})$
IV	255	3.92 (52 500)	c 3.80 (−4.96); 3.96 (0); 4.10 (+3.48)	$E_u(a^1E_u)$
			4.48 (−0.48)	Br^- CTTS
V	198	5.05 (17 400)	4.94 (−2.66)	Br^- CTTS
		$[(n\text{-}C_4H_9)_4N][Au(CN)_2Cl_2]$		
I	292	3.42 (1060)	3.37 (+0.27)	$B_{3u}(^1B_{3u})$
			3.85 (−0.18)	$B_{1u}(^1B_{1u})$
II	220	4.55 (21 400)	4.49 (−0.76)	$B_{2u}(^1B_{2u})$
III	204[b]	4.90 (13 700)	4.94 (+1.10)	$B_{2u}(CN^-)$
		$[(n\text{-}C_4H_9)_4N][Au(CN)_2Br_2]$		
I	357[b]	2.80 (650)	2.76 (+0.16)	$B_{3u}(^1B_{3u})$
II	325	3.08 (840)	3.10 (−0.09)	$B_{1u}(^1B_{1u})$
III	241	4.15 (29 000)	4.24 (−0.29)	$B_{2u}(^1B_{2u})$
IV	209	4.78 (13 600)	4.70 (+0.87)	$B_{2u}(CN^-)$
V	202	4.95 (14 100)	5.06 (−0.67)	Br^- CTTS
		$[(n\text{-}C_4H_9)_4N][Au(CN)_2I_2]$[d]		
I	444[b]	2.25 (920)	2.19 (+0.10)	$B_{3u}(^1B_{3u})$
II	375	2.67 (5800)	2.50 (−0.16)	$B_{1u}(^1B_{1u})$
III	272	3.67 (41 700)	e	$B_{2u}(^1B_{2u})$
IV	237	4.22 (19 400)[f]		$B_{2u}(CN^-)$
V	213[b]	4.70 (21 700)[f]		I^- CTTS
VI	203	4.92 (33 900)[f]		I^- CTTS
		$[(CH_3)_4N][Au(CN)_2ClBr]$		
I	345[b]	2.90 (400)		$B_1(^1B_1)$
II	306	3.27 (675)		$A_1(^1A_1)$
III	235	4.25 (18 500)		$B_2(^1B_2)$
IV	209	4.78 (12 000)		$B_2(CN^-)$
		$[(n\text{-}C_4H_9)_4N][Au(CN)_2BrI]$[d]		
I	373	2.68 (1840)		$B_1(^1B_1)$, $A_1(^1A_1)$
II	257	3.89 (25 000)		$B_2(^1B_2)$
III	240	4.18 (15 000)[f]		$B_2(CN^-)$
IV	212[b]	4.72 (16 800)[f]		Br^-, I^- CTTS
V	204[b]	4.90 (23 500)[f]		Br^-, I^- CTTS

[a] Acetonitrile solution. [b] Shoulder. [c] *A* term. [d] Corrected for dissociation (see text). [e] Signal too weak to measure: <0.06 $(M\ cm\ T)^{-1}$. [f] Accuracy may be lower due to strong absorption by dissociation products.

Discussion

Spectral Assignments and Interpretation. Two intense band systems are observed in the spectra of each halo Au(III) complex. The lower energy system is weaker and for bromo or iodo complexes shows a shoulder on the low-energy side of the band maximum. These two band systems can be interpreted by the LMCT model as transitions from the halogen π and, in the case of AuX_4^-, nonbonding MO's (lower energy systems) and from the halogen σ MO's (higher energy systems) to the predominantly Au $5d_{x^2-y^2}$ σ^* orbital, $2b_{1g}(x^2 - y^2)$ or $4a_g(x^2 - y^2)$. Table IV lists the individual LMCT assignments for each complex. The lower intensity of the π

and n $\rightarrow \sigma^*$ LMCT is consistent with the smaller electric dipole transition moments discussed above and limited σ–π intermixing. The higher energy $\sigma \rightarrow \sigma^*$ LMCT band in every case is very intense.

The extent of σ–π mixing for the AuX_4^- complexes can be determined from the MCD spectra by using eq 11. For $AuCl_4^-$ spin–orbit coupling is small and therefore the $\sigma \rightarrow \sigma^*$ LMCT band to a good approximation will be $^1A_{1g} \rightarrow a^1E_u$. In this case $e_i \simeq 1$, all other spin–orbit coefficients $\simeq 0$, and eq 11 simplifies to $A_1 = 2\lambda_1\lambda_2 D_0(^1E_u)$. In the absence of σ–π mixing ($\lambda_1 = 1$ and $\lambda_2 = 0$) the magnitude of the A_1 term will be determined by several two-center integrals that are expected to be extremely small. The clearly observed positive A_1 term for band III in the $AuCl_4^-$ spectrum therefore implies significant σ–π mixing. A moment analysis of band III provides the value of $A_1/D_0 = +0.44$, which leads to an estimate of $\lambda_1 = 0.98$ and $\lambda_2 = 0.23$. The sign of the A_1 term for band III is also consistent with the prediction of eq 11.

The lower energy $\pi \rightarrow \sigma^*$ transition for $AuCl_4^-$, $^1A_{1g} \rightarrow b^1E_u$, should also exhibit an A_1 term but of the opposite sign. If spin–orbit coupling from the Cl^- ligand is ignored, once again eq 11 reduces to ($b_i \simeq 1$ and all other spin–orbit coefficients $\simeq 0$) $A_1 = -2\lambda_1\lambda_2 D_0(^1E_u)$ if the only significant source of intensity for the $\pi \rightarrow \sigma^*$ transition is via σ–π mixing. The values of λ_1 and λ_2 are such that the negative A_1 term would be only about 6% as large as the A_1 term for the $\sigma \rightarrow \sigma^*$ transition. The observed MCD in the region of band I for $AuCl_4^-$ is predominantly a positive B_0 term, which would likely obscure such a weak A_1 term. A moment analysis of band I did reveal a small negative A_1 component, but since more than one transition is expected beneath band I, the interpretation of this result as due to $^1A_{1g} \rightarrow b^1E_u$ alone is difficult. It may be noted here that an earlier high-resolution MCD study of $AuCl_4^-$ doped into a Cs_2NaYCl_6 lattice revealed a progression of lattice vibrations at 10 K built on a sharp electronic origin at 3.062 μm^{-1}, which exhibited a *positive* A_1 term.[11] As a consequence of the A_1 term the electronic transition was assigned as $^1A_{1g} \rightarrow b^1E_u$. As eq 11 and its simplified form show, the *positive* A_1 term is not consistent with this LMCT assignment. However, the position of the origin on the low-energy side of band I suggests the possibility of an E_u state associated with a spin-forbidden transition. In this context the $E_u(^3A_{2u})$ state is predicted by eq 11 to have a positive A_1 term, although a transition to this state is expected to be quite weak. Thus, the assignment of the sharp origin at 3.062 μm^{-1} should be reconsidered.

The interpretation of the large positive B_0 term for band I in the $AuCl_4^-$ spectrum is less straightforward because of the summations involved and the evaluation of the dipole integrals $D(^1E_u)$ and $D(^1A_{2u})$ of eq 13 and 14. These latter integrals are two centered and are difficult to evaluate exactly. However, from overlap considerations some rough estimates were made. These estimates together with the values of λ_1 and λ_2 and the assumption that the $\sigma \rightarrow \sigma^*$ $|D(^1E_u)| >>$ n $\rightarrow \sigma^*$ $|D(^1A_{2u})|$ lead to the conclusion that the largest contribution to the B_0 term for band I is the interaction of b^1E_u with a^1E_u, giving rise to a positive term for b^1E_u (band I) and a negative term for a^1E_u (band III). The B_0 term for the $^1A_{2u}$ state was found to be much smaller by comparison and to be of uncertain sign due to summation of contributions of nearly the same magnitude but of opposite sign. Our analysis of the B_0 term contributions to band I is necessarily crude in view of the approximations involved, but it does lead to a prediction of a positive B_0 term for band I, consistent with experiment.

In the case of $AuBr_4^-$ spin–orbit coupling due to Br^- was carefully considered, but model calculations showed that the energy splitting of the E_u and A_{2u} spin–orbit states was relatively small and intermixing of singlet and triplet states in the spin–orbit eigenvectors was not extensive. As can be seen in the secular determinants of Table III, the σ–π mixing coefficients λ_1 and λ_2 serve to reduce the spin–orbit interaction in a number of the matrix elements. This feature together with the substantial energy separations between the $\sigma \rightarrow \sigma^*$ and the n or $\pi \rightarrow \sigma^*$ LMCT states nullifies a strong spin–orbit perturbation of the LMCT spectra. The shoulder (band I) resolved on the low-energy side of band II may be due to transitions that are formally of spin-forbidden parentage, but the lack of further resolution precludes a more detailed analysis. Model spin–orbit calculations suggest assignments to $E_u(^3A_{2u})$, $A_{2u}(^3E_u)$, and $E_u(^3E_u)$ states as reasonable possibilities, but their singlet character is predicted to be relatively small. The observation of the prominent positive A_1 term for the $A_{1g} \rightarrow E_u(a^1E_u)$ transition (band IV) at 3.92 μm^{-1} in the $AuBr_4^-$ MCD spectrum can be interpreted in the same way as band III for $AuCl_4^-$. Moment analysis gave $A_1/D_0(^1E_u) = +0.38$, leading to $\lambda_1 = 0.98$ and $\lambda_2 = 0.20$, values which are quite comparable to those for $AuCl_4^-$. Similarly, the lack of an observed negative A_1 term for the $A_{1g} \rightarrow E_u(b^1E_u)$ is based on the same intensity argument presented for $AuCl_4^-$.

For both the $AuCl_4^-$ and $AuBr_4^-$ ions a weak shoulder is observed on the low-energy side of the intense $\sigma \rightarrow \sigma^*$ LMCT band (band II at 3.80 μm^{-1} for $AuCl_4^-$ and band III at 3.30 μm^{-1} for $AuBr_4^-$) with weak corresponding features in the MCD. These weak bands, which have not been reported previously, are difficult to assign. Their low intensity is indicative of a forbidden transition. However, it seems unlikely that they are due to the spin-forbidden LMCT to $E_u(a^3E_u)$ or $A_{2u}(a^3E_u)$ because the greater spin–orbit coupling of Br^- compared to Cl^- would predict greater singlet character and therefore greater intensity for the transition for $AuBr_4^-$ whereas just the opposite is observed. Two other possible assignments are to a ligand field (LF) transition or to a transition to the orbitally forbidden $^1B_{2u}$ LMCT state. Each of these assignments has difficulties. The bands are too intense for a LF assignment unless their close proximity to the intense $\sigma \rightarrow \sigma^*$ enhances their intensity by vibronic coupling. Further the LF assignment would place the LF state some 1.2–1.4 μm^{-1} higher in energy than the lowest energy observed LF state for $AuCl_4^-$ or $AuBr_4^-$.[10] This latter consideration leads to a rather large splitting of the occupied Au(III) 5d orbitals. The assignment to a transition to the $^1B_{2u}$ LMCT state would place an out-of-plane $\pi \rightarrow \sigma^*$ state some 0.7–0.8 μm^{-1} higher in energy than the in-plane $\pi \rightarrow \sigma^*$ state (b^1E_u). Such a large difference in energy between the two π ligand MO's is difficult to explain. Although we favor the $^1B_{2u}$ LMCT assignment over the LF assignment, it must be admitted that the present results cannot provide definitive support for either. Further study of these weak features including their temperature dependence would be desirable. If the $^1B_{2u}$ LMCT assignment is adopted, then an additional weak feature observed in the MCD of $AuBr_4^-$ at 3.04 μm^{-1} may be assigned tentatively as the formally spin-forbidden transition to $E_u(^3B_{2u})$. The corresponding transition for $AuCl_4^-$ would be expected to be weaker and therefore obscured by the large positive B_0 term of band II.

In reference to the *trans*-$Au(CN)_2X_2^-$ complexes, the MCD spectra in the region of the lower energy $\pi \rightarrow \sigma^*$ LMCT show two B_0 terms of opposite signs in each case, with the positive term at lowest energy. An analysis of the B_0 terms expected for the $\pi \rightarrow \sigma^*$ transitions $A_g \rightarrow B_{1u}(^1B_{1u})$ and $A_g \rightarrow B_{3u}(^1B_{3u})$ using expressions such as eq 14 and 15 with dipole terms approximated as before predicts a positive B_0 term for the transition to the B_{3u} state in the absence of strong spin–orbit coupling, provided the B_{3u} state is lower in energy than the B_{1u} state. Consideration of spin–orbit coupling did not change this prediction. Similarly, a negative B_0 term is predicted in each case for the transition to the B_{1u} state. The B_0 term for

the higher energy $\sigma \rightarrow \sigma^*$ transition $A_g \rightarrow B_{2u}(^1B_{2u})$ is also predicted to be negative. These predictions lead to the order of these states reflected in the assignments of Table IV.

The spectra of the *trans*-$Au(CN)_2X_2^-$ ions also exhibit an intense high-energy band (band III for X = Cl^- and band IV for X = Br^- or I^-) that has no counterpart in the spectra of AuX_4^- and cannot be explained in terms of halide LMCT. For *trans*-$Au(CN)_2Br_2^-$ and *trans*-$Au(CN)_2Cl_2^-$ positive B_0 terms corresponding to these bands are observed in the MCD. These bands are tentatively assigned to $\pi(CN^-) \rightarrow \sigma^*$, LMCT involving the occupied π orbitals of the cyano ligands. In view of the intensities, the excited states are likely of B_{2u} symmetry ($1b_{2u}' \rightarrow 4a_g(x^2 - y^2)$) because $\sigma-\pi$ mixing of the CN^- π orbital ($1b_{2u}$) with the halide σ orbital ($2b_{2u}$) via eq 3 would provide $\sigma \rightarrow \sigma^*$ character to the transition. The corresponding LMCT transition in $Au(CN)_4^-$ must occur at higher energy than for the *trans*-$Au(CN)_2X_2^-$ ions because no maxima or shoulders are observed below 5.2 μm^{-1}.[10] A red shift in CN^- LMCT for *trans*-$Au(CN)_2X_2^-$ is reasonable because the halide ligands are expected to be poorer σ donors than CN^-, resulting in a more stable σ^* orbital ($4a_g(x^2 - y^2)$ of Figure 1).

Bands in the spectra of $AuBr_4^-$ (band V at 5.05 μm^{-1} and also bands at 4.48 and 4.94 μm^{-1} in the MCD), *trans*-$Au(CN)_2Br_2^-$ (band V at 4.95 μm^{-1}), and *trans*-$Au(CN)_2I_2^-$ (bands V at 4.70 μm^{-1} and VI at 4.92 μm^{-1}) have not yet been assigned. These bands are all quite intense, characteristic of allowed transitions, but they cannot be interpreted within the LMCT model. They occur at high energy in a region where free halide ions are known to exhibit intense bands. For example Br^- in acetonitrile has intense bands with maxima at 4.59 μm^{-1} (ϵ 10 700) and 4.93 μm^{-1} (ϵ 10 600) while I^- has bands with maxima at 4.08 μm^{-1} (ϵ 16 300) and 4.88 μm^{-1} (ϵ 22 000).[22] These spectra are sensitive to the nature of the solvent and have been assigned to a process described as charge transfer to solvent (CTTS).[22-24] The spectra of the $AuBr_4^-$ and *trans*-$Au(CN)_2Br_2^-$ in water do show some differences from spectra in acetonitrile in this high-energy region, but difficulties due to hydrolysis cannot be ruled out entirely. Suppression of hydrolysis by adding excess halide ion obscures the changes of interest. The dissociation equilibrium for *trans*-$Au(CN)_2I_2^-$ likewise makes measurements in this region uncertain. However, on the basis of their energy and intensity, the high-energy bands in the halo Au(III) complexes are tentatively assigned as CTTS. The MCD for $AuBr_4^-$ and *trans*-$Au(CN)_2Br_2^-$ (band V in each case) is qualitatively consistent with that reported for Br^- CTTS in acetonitrile.[22]

The spectral assignments of the *trans*-$Au(CN)_2BrY^-$ ions given in Table IV are made by analogy to the *trans*-$Au(CN)_2X_2^-$ ions. The symmetry representations are given for their lower molecular symmetry (C_{2v}), but these representations are easily correlated with those of D_{2h}. The bands in these mixed-halo complexes are intermediate in energy between *trans*-$Au(CN)_2Br_2^-$ and *trans*-$Au(CN)_2Y_2^-$ (Y = Cl^-, I^-).

General Trends in LMCT Spectra. In terms of general trends among the halo Au(III) LMCT spectra, the characteristic energy shifts of corresponding bands in the order $Cl^- > Br^- > I^-$ are observed. This "hallmark" order of LMCT follows the stability of the occupied halide orbitals and depends to a lesser extent on differences in halide σ bonding, which affect the σ^* orbital stability. The energy shifts $Au(CN)_4^-$ > *trans*-$Au(CN)_2X_2^-$ > AuX_4^- for corresponding LMCT bands is also a feature of the Au(III) spectra and can be rationalized by the increase in stability of the σ^* orbital as the strong σ donor CN^- is replaced by a weaker σ-donor halide. When the $\pi \rightarrow \sigma^*$ and $\sigma \rightarrow \sigma^*$ energy differences for AuX_4^- and *trans*-$Au(CN)_2X_2^-$ are compared, it is interesting that the energy difference between these two types of transitions is greater for AuX_4^- (1.31 μm^{-1} for Cl^- and 1.38 μm^{-1} for Br^-) than for *trans*-$Au(CN)_2X_2^-$ (1.13 μm^{-1} and 1.07 μm^{-1} for Br^-). The greater difference for AuX_4^- may reflect the $\sigma-\pi$ intermixing between the halide σ- and π-bonding MO's ($1e_u$ and $2e_u$), which will serve to separate them. In contrast, the $\sigma-\pi$ mixing in *trans*-$Au(CN)_2X_2^-$ involves mixing between the halide orbitals and more stable CN^- orbitals, which is likely less extensive and serves to destabilize both the σ and π halide orbitals. It must be admitted however that the differences are not large and may also reflect electron-repulsion differences between the two types of complexes.

Acknowledgment is made to the donors of the Petroleum Research Fund, administered by the American Chemical Society, for support of this research. H.I. also acknowledges the Scientific and Technical Research Council of Turkey for a fellowship and the Middle East Technical University for a leave of absence.

Registry No. $AuCl_4^-$, 14337-12-3; $AuBr_4^-$, 14337-14-5; *trans*-$Au(CN)_2Cl_2^-$, 39048-42-5; *trans*-$Au(CN)_2Br_2^-$, 30869-88-6; *trans*-$Au(CN)_2I_2^-$, 39043-93-1; *trans*-$Au(CN)_2BrCl^-$, 30869-89-7; *trans*-$Au(CN)_2BrI^-$, 86088-79-1.

(22) El-Kourashy, A.-G.; Grinter, R. *J. Chem. Soc., Faraday Trans. 2* **1977**, *73*, 1050.
(23) Fox, M. F.; Hayon, E. *J. Chem. Soc., Faraday Trans. 1* **1977**, *73*, 872; **1978**, *74*, 1003.
(24) Fox, M. F.; Barker, B. E.; Hayon, E. *J. Chem. Soc., Faraday Trans. 1* **1978**, *74*, 1776.

Contribution from Bell Laboratories,
Murray Hill, New Jersey 07974

Photooxidation of Trichlorosilane in Silicon Tetrachloride

ROBERT GOODEN

Received September 17, 1982

Trichlorosilanol, Cl_3SiOH, was formed by low-pressure mercury-lamp photolysis of trichlorosilane, Cl_3SiH, and oxygen in silicon tetrachloride. This conversion was quantitative at low silane concentrations (200–2500 ppm) and was used to determine an infrared absorptivity at 3680 cm^{-1} of 102 ± 5 L/(mol cm) for Cl_3SiOH, a very reactive impurity in $SiCl_4$ that is unavailable in pure form. The high quantum efficiency (≥285) indicated a radical-chain pathway for the reaction. The hydroperoxide Cl_3SiOOH was not detected even under low-temperature photolysis where it should be thermally stable and was not likely to be a significant intermediate.

Introduction

The determination and removal of impurities from reactive compounds present interesting challenges in analysis and purification. The highly reactive and sensitive halides of silicon and germanium are used to fabricate optical waveguide glass fibers via the modified chemical vapor deposition (MCVD)

0020-1669/83/1322-2272$01.50/0